"Mixing Rules" for Estimating the Hydraulic Permeability of Fiber Mixtures

Kristin J. Mattern and William M. Deen
Dept. of Chemical Engineering, Massachusetts Institute of Technology, Cambridge, MA 02139

DOI 10.1002/aic.11350
Published online November 20, 2007 in Wiley InterScience (www.interscience.wiley.com).

While theoretical results for the hydraulic permeability of fibrous media are typically based on a single type of fiber in an ordered array, many synthetic or biological materials are composed of fibers which differ in size, charge, orientation, or other characteristics. It is desirable to be able to estimate the permeability of such a mixture from its composition and the properties of the individual fiber types. Toward that end, we compared four "mixing rules" proposed in the literature, each based on differing approximations of the hydrodynamic interactions between multiple fiber types. To provide data for charged fibers, the open-circuit hydraulic permeabilities of periodic arrays of fibers with different surface charge densities and/or radii were computed using finite element methods. Based on these data for charged fibers, as well as published results for arrays of uncharged fibers of differing radii and/or orientation, we compared the four mixing rules for 64 cases. In some situations there were several-fold differences among the predicted hydraulic permeabilities. Nonetheless, a volume-weighted averaging of the resistivities of individual fiber types was found to be reasonably reliable, giving an overall root-mean-square error of 24%. This mixing rule was equally applicable to systems containing charged or neutral fibers. © 2007 American Institute of Chemical Engineers *AIChE J,* 54: 32–41, 2008
Keywords: fibers, fluid mechanics, Darcy permeability, electrokinetics

Introduction

Viscous flow through porous media is customarily modeled by using Darcy's law to relate the velocity ($\langle \mathbf{v} \rangle$) to the pressure gradient ($\langle \nabla P \rangle$). For an isotropic material,

$$\langle \mathbf{v} \rangle = -\frac{\kappa}{\mu} \langle \nabla P \rangle \tag{1}$$

where μ is the viscosity and κ is the Darcy permeability. The velocity and pressure are each averaged over a volume that is large compared to the microstructural features (e.g., grain or pore size) but small compared to the system, making Eq. 1 both macroscopic and local. Such averaging is denoted by the angle brackets. Implicit in Eq. 1 is the assumption that inertia is absent; that is, the Reynolds number based on the microstructural length scale is very small. With μ factored out (as shown), and in the absence of any effects of electrical charge, the coefficient κ depends solely on the microstructural geometry.

Among the situations where Darcy's law is applicable is the pressure-driven, creeping flow of liquids through fibrous materials. Examples include cellulosic membranes, polymeric hydrogels such as agarose, and certain body tissues. In such materials the fibers are either single polymer chains or multichain aggregates, and are typically cross-linked. Often, the fibers are not identical, differing in size, electrical charge, and/or other characteristics. This is true especially in physiological systems, such as glomerular basement membrane,[1,2] cartilage,[3] and other tissues,[4] which contain a mixture of structural biopolymers. The

Correspondence concerning this article should be addressed to W. M. Deen at wmdeen@mit.edu.

problem we address is how to use hydrodynamic models to estimate κ for such a mixture, if the properties of each fiber type are known.

A variety of models have been used to predict the Darcy permeability of fibrous media, based on Stokes flow through arrays of cylinders. The simplest situations, which yield analytical results, are spatially periodic, parallel arrays of uncharged fibers of uniform radius, with flow either perpendicular to the fiber axes (transverse flow) or parallel to the axes (axial flow).[5–7] Periodic arrays of charged fibers of uniform size and charge density have been analyzed computationally.[8] Numerical results have been reported also for randomly oriented arrays of a single type of uncharged fiber.[9–11] Results for fiber mixtures are much more limited. For arrays of uncharged fibers having two different radii, there are numerical results for periodic arrangements of parallel fibers[12] and for randomly oriented fibers.[10] Analytical results were derived for a situation in which the radii and volume fractions are such that the fine fibers form a homogeneous region between the coarse fibers.[13] There appear to be no results for mixtures of charged fibers of differing size or charge density.

The main difficulty in estimating κ for fiber mixtures is that the hydraulic resistances of the subpopulations are interdependent, even for dilute systems. This is evident in the analytical results for uniform cylinders or fibers. If resistances in a dilute fiber array were simply additive, then the resistivity ($1/\kappa$) would become proportional to the solid volume fraction (ϕ) as $\phi \to 0$. Actually, $1/\kappa$ varies as $-\phi/\ln \phi$ in this limit,[5,7] a consequence of the long-range hydrodynamic interactions in Stokes flow. Thus, there is no simple and rigorous way to estimate κ for fiber mixtures, even if the volume fraction of each fiber type is arbitrarily small. Several expressions, which we term *mixing rules*, have been proposed to predict the permeability of systems with a mixture of fiber radii[4,10] or a mixture of fiber orientations[14,15] from models based on fibers of one type. However, their comparative accuracy has not been investigated systematically.

Insight into the origins of the various mixing rules is provided by a force balance on a small sample of fibrous medium of total volume V, containing liquid and a mixture of two types of fibers. For simplicity, the flow is assumed to be unidirectional at the macroscopic (Darcy) length scale, with the magnitude of the velocity denoted as v. Equating the pressure force on the fluid with the force that the fluid exerts on the fibers, and using Eq. 1, gives

$$\frac{1}{\kappa} = \frac{F_1 + F_2}{\mu \langle v \rangle V} \tag{2}$$

where F_1 and F_2 are the total forces acting on fibers of types 1 and 2, respectively. Letting r_i and ϕ_i be the radius and volume fraction, respectively, of fibers of type i, the dimensionless force per fiber length is defined as

$$f_i = \frac{\pi r_i^2 F_i}{\phi_i \mu \langle v \rangle V}. \tag{3}$$

This allows the Darcy resistivity to be expressed as

$$\frac{1}{\kappa} = \frac{\phi_1 f_1}{\pi r_1^2} + \frac{\phi_2 f_2}{\pi r_2^2}. \tag{4}$$

Although it appears here that the contributions of the two-fiber populations to the resistivity are simply additive, one must keep in mind that f_1 and f_2 are each functions of both ϕ_1 and ϕ_2, because of the long-range hydrodynamic interactions among fibers.

For a single population of fibers of radius r and volume fraction ϕ, Eq. 4 rearranges to

$$\frac{f}{\pi r^2} = \frac{1}{\phi \kappa(\phi)} \tag{5}$$

where the function $\kappa(\phi)$ applies to a particular fiber orientation, radius, and charge density. For one fiber type in a mixture of total fiber volume fraction ϕ, the question arises as to whether the equivalent expression should be

$$\frac{f_i}{\pi r_i^2} = \frac{1}{\phi \kappa_i(\phi)} \tag{6}$$

or

$$\frac{f_i}{\pi r_i^2} = \frac{1}{\phi_i \kappa_i(\phi_i)}. \tag{7}$$

In other words, should the force per unit length for fiber type i be based on ϕ or ϕ_i? Both expressions have a certain plausibility, although neither is likely to be exactly correct.

If Eq. 6 is substituted into Eq. 4, the result is what we term a *volume-weighted resistivity*:

$$\frac{1}{\kappa} = \frac{\phi_1}{\phi} \frac{1}{\kappa_1(\phi)} + \frac{\phi_2}{\phi} \frac{1}{\kappa_2(\phi)}. \tag{8}$$

This mixing rule was proposed by Clague and Phillips[10] for fiber mixtures with differing radii. Alternatively, if Eq. 7 is substituted into Eq. 4, the result is an *unweighted resistivity*:

$$\frac{1}{\kappa} = \frac{1}{\kappa_1(\phi_1)} + \frac{1}{\kappa_2(\phi_2)}. \tag{9}$$

This is equivalent to what was used by Jackson and James[6,14] to estimate the permeability of randomly oriented fibers of uniform size, where two-thirds of the fibers were envisioned as experiencing transverse flow and one-third axial flow.

There are many more possibilities, two of which appear in the literature and are considered here. A development by Ethier[4,16] led to a *length-weighted resistivity*:

$$\frac{\left(\phi_1 / r_1^2\right) + \left(\phi_2 / r_2^2\right)}{\kappa} = \frac{\left(\phi_1 / r_1^2\right)}{\kappa_1(\phi)} + \frac{\left(\phi_2 / r_2^2\right)}{\kappa_2(\phi)}. \tag{10}$$

Here, the terms in the numerators are proportional to the total lengths of each fiber type. Finally, there is a *volume-weighted permeability*:

$$\kappa = \frac{\phi_1}{\phi} \kappa_1(\phi) + \frac{\phi_2}{\phi} \kappa_2(\phi) \tag{11}$$

which was used to find the permeability of randomly oriented, charged fibers from results for parallel, periodic arrangements.[8,15]

To assess the accuracy of the four mixing rules, we compared the Darcy permeabilities predicted by each to those computed in the literature for a variety of situations, including parallel or randomly oriented single-fiber and two-fiber systems. To provide more data for charged fibers, finite element calculations were performed for periodic arrays of fibers with different surface charges and/or radii, and these new results were also used to test the mixing rules. As will be shown, Eq. 8 was found to be the most reliable of the four.

Model Development

General features of charged fiber arrays

Flow through arrays of charged fibers is influenced by electrical potentials, because each fiber is surrounded by a diffuse double layer which contains a net charge that is opposite to that on the fiber surface. Thus, an applied or induced electric field produces an electrical body force. Another consequence of the fluid having a net charge is that the pressure-driven flow can create an electric current. The relationships between hydrodynamic and electrical phenomena are embodied in a set of electrokinetic coupling coefficients (k_{ij}), which relate the area-averaged velocity ($\langle \mathbf{v} \rangle$) and area-averaged current density ($\langle \mathbf{j} \rangle$) to the macroscopic gradients in pressure and electrical potential (Ψ). The linear force–flux relationships are

$$\begin{bmatrix} \langle \mathbf{v} \rangle \\ \langle \mathbf{j} \rangle \end{bmatrix} = \begin{bmatrix} -k_{11} & k_{12} \\ k_{21} & -k_{22} \end{bmatrix} \begin{bmatrix} \langle \nabla P \rangle \\ \langle \nabla \Psi \rangle \end{bmatrix} \tag{12}$$

where k_{11} (short-circuit hydraulic permeability) and k_{22} (electrical conductivity) are both positive. The off-diagonal coefficients each have the same sign as the fixed charge (i.e., the charge on the fiber surface) and, by Onsager reciprocity, $k_{12} = k_{21}$.[17] For pressure-driven flow under open-circuit conditions (zero net current), the apparent hydraulic permeability is

$$k_{oc} = k_{11} - \frac{k_{12}k_{21}}{k_{22}}. \tag{13}$$

Thus, the open-circuit permeability (k_{oc}) is always less than the short-circuit value; k_{11} in turn is less than or equal to that for an identical array of uncharged fibers. Accordingly, under open-circuit conditions, electrokinetic coupling always retards the flow. All Darcy permeabilities reported here are open-circuit values ($\kappa = \mu k_{oc}$).

Model geometry

Spatially periodic arrays containing two types of fibers were modeled, as shown in Figure 1a. The side length of the square unit cell was $2B$, and there were equal numbers of the two-fiber types, each characterized by a volume fraction (ϕ_i), a radius (r_i), and a surface charge density (σ_i). The unit cell width is related to the radius and volume fraction of each fiber by

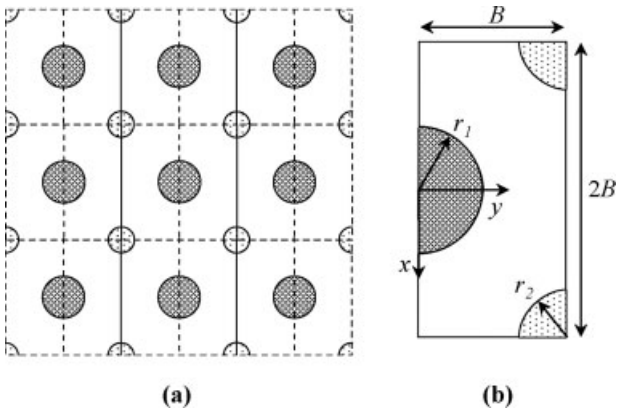

Figure 1. (a) Periodic array of two fiber types, with boundaries of square unit cells. (b) Computational domain for fibers with radii r_1 and r_2 and unit cell width B.

Pressure or electrical potential gradients were imposed either in the x direction (transverse flow) or the z direction (axial flow, normal to the page).

$$B = r_i\sqrt{\frac{\pi}{4\phi_i}}. \tag{14}$$

In the transverse flow problem, there were local velocities $v_x(x,y)$ and $v_y(x,y)$, but with net flow only in the x direction. In the axial flow problem, there was just one nonvanishing velocity component, $v_z(x,y)$. Because in either situation $y = 0$ and $y = B$ were symmetry planes, and because the variations in velocity and ion concentrations with x were periodic, it was sufficient to consider the half-cell shown in Figure 1b.

Problem formulation

It was assumed that the electrolyte solution contained one type each of univalent cation and univalent anion. Accordingly, there were five dimensional field variables: pressure (P), velocity ($\mathbf{v}$), molar concentrations of the two ions ($C_\pm$), and electrical potential (Ψ). The steady-state system of partial differential equations included the Navier–Stokes equation with electrical body force, the continuity equation, species conservation equations for cations and anions, and Poisson's equation:

$$\nabla P = \mu\nabla^2\mathbf{v} + \varepsilon\nabla^2\Psi\nabla\Psi \tag{15}$$

$$0 = \nabla\cdot\mathbf{v} \tag{16}$$

$$0 = \nabla\cdot\left(-D_i\nabla C_i - \frac{z_iD_iF}{RT}C_i\nabla\Psi + C_i\mathbf{v}\right) = \nabla\cdot\mathbf{N}_i \tag{17}$$

$$\nabla^2\Psi = \frac{F}{\varepsilon}\left(C_- - C_+\right) \tag{18}$$

Here, C_i is the concentration of species i, $\mathbf{N}_i$ is its flux (given by the Nernst–Planck equation), D_i is its diffusivity, z_i ($=\pm 1$) is its valence, ε is the dielectric permittivity of the solvent, R is the gas constant, T is absolute temperature, and F is Faraday's constant.

Dimensionless variables were defined using the Debye length (λ), superficial velocity (v_0), bulk (external) salt concentration (C_0), bulk osmotic pressure ($\Pi_0 = 2RTC_0$), and thermal voltage ($\Psi_0 = RT/F$) as scales. The resulting variables were $\tilde{\Psi} = \Psi/\Psi_0$, $\tilde{C}_\pm = C_\pm/C_0$, $\tilde{\mathbf{N}}_\pm = \mathbf{N}_\pm\lambda/D_\pm C_0$, $\tilde{P} = P/\Pi_0 = P/2RTC_0$, and $\tilde{\mathbf{v}} = \mathbf{v}/v_0$. For a univalent–univalent electrolyte, the Debye length is given by

$$\lambda = \sqrt{\frac{\varepsilon RT}{2F^2C_0}}. \tag{19}$$

The dimensionless forms of the differential equations were

$$\tilde{\nabla}\tilde{P} = \beta\tilde{\nabla}^2\tilde{\mathbf{v}} + \tilde{\nabla}^2\tilde{\Psi}\,\tilde{\nabla}\tilde{\Psi}. \tag{20}$$

$$0 = \tilde{\nabla}\cdot\tilde{\mathbf{v}} \tag{21}$$

$$0 = \tilde{\nabla}\cdot\left(-\tilde{\nabla}\tilde{C}_+ - \tilde{C}_+\tilde{\nabla}\tilde{\Psi} + \beta\alpha\tilde{C}_+\tilde{\mathbf{v}}\right) = \tilde{\nabla}\cdot\tilde{\mathbf{N}}_+ \tag{22}$$

$$0 = \tilde{\nabla}\cdot\left(-\tilde{\nabla}\tilde{C}_- + \tilde{C}_-\tilde{\nabla}\tilde{\Psi} + \beta\alpha\frac{D_+}{D_-}\tilde{C}_-\tilde{\mathbf{v}}\right) = \tilde{\nabla}\cdot\tilde{\mathbf{N}}_- \tag{23}$$

$$\nabla^2\tilde{\Psi} = \frac{1}{2}\left(\tilde{C}_- - \tilde{C}_+\right) \tag{24}$$

These governing equations contain two dimensionless groups,

$$\beta = \frac{v_0\mu\lambda}{\varepsilon\Psi_0^2} = \frac{(v_0\mu/\varepsilon\Psi_0)}{(\Psi_0/\lambda)} \tag{25}$$

which is the strength of the flow-induced electric field relative to that in an equilibrium double layer, and

$$\alpha = \frac{\varepsilon\Psi_0^2}{\mu D_+} = \left(\frac{v_0\lambda}{D_+}\right)\left(\frac{1}{\beta}\right) \tag{26}$$

which is the Peclet number for the cation divided by β.

Zeroth-order perturbation solution

For a typical superficial velocity (v_0) of 10^{-7} m/s and an aqueous 0.1 M salt solution, the orders of magnitude of the dimensionless groups are $\beta \sim 10^{-7}$ and $\alpha \sim 1$, which suggests a perturbation expansion in β. The resulting perturbation problem is regular, with $\beta = 0$ corresponding to equilibrium double layers. Accordingly, the five field variables were each expressed as power series in β. For example, the series for the potential was

$$\tilde{\Psi} = \tilde{\Psi}^{(0)} + \beta\tilde{\Psi}^{(1)} + O(\beta^2). \tag{27}$$

The differential equations for the zeroth and first-order problems will be given first, and then the boundary conditions will be summarized.

As already indicated, the zeroth-order solution corresponds to the case of no flow. This uncouples the species conservation and Poisson equations from the equations of motion. The ion concentrations at equilibrium follow Boltzmann distributions

$$\tilde{C}_\pm^{(0)} = \exp(\mp\tilde{\Psi}^{(0)}) \tag{28}$$

and the potential is governed by the Poisson–Boltzmann equation,

$$\tilde{\nabla}^2\tilde{\Psi}^{(0)} = \sinh\tilde{\Psi}^{(0)}. \tag{29}$$

Equations 28 and 29 provide first approximations to the concentration and potential fields for both transverse and axial flow. As will be seen, the equilibrium pressure field ($\tilde{P}^{(0)}$) is not needed.

First-order perturbation for transverse flow

Substituting the expansions into Eqs. 20–24 and retaining terms of $O(\beta)$, the first-order perturbation problem for transverse flow was found to be governed by

$$\tilde{\nabla}\tilde{P}^{(1)} = \tilde{\nabla}^2\tilde{\mathbf{v}}^{(0)} + \tilde{\nabla}^2\tilde{\Psi}^{(1)}\,\tilde{\nabla}\tilde{\Psi}^{(0)} + \tilde{\nabla}^2\tilde{\Psi}^{(0)}\,\tilde{\nabla}\tilde{\Psi}^{(1)} \tag{30}$$

$$0 = \tilde{\nabla}\cdot\tilde{\mathbf{v}}^{(0)} \tag{31}$$

$$0 = \tilde{\nabla}\cdot\left(-\tilde{\nabla}\tilde{C}_+^{(1)} - \tilde{C}_+^{(0)}\tilde{\nabla}\tilde{\Psi}^{(1)} - \tilde{C}_+^{(1)}\tilde{\nabla}\tilde{\Psi}^{(0)} + \alpha\tilde{C}_+^{(0)}\tilde{\mathbf{v}}^{(0)}\right) = \tilde{\nabla}\cdot\tilde{\mathbf{N}}_+^{(1)} \tag{32}$$

$$0 = \tilde{\nabla}\cdot\left(-\tilde{\nabla}\tilde{C}_-^{(1)} + \tilde{C}_-^{(0)}\tilde{\nabla}\tilde{\Psi}^{(1)} + \tilde{C}_-^{(1)}\tilde{\nabla}\tilde{\Psi}^{(0)} + \alpha\frac{D_+}{D_-}\tilde{C}_-^{(0)}\tilde{\mathbf{v}}^{(0)}\right) = \tilde{\nabla}\cdot\tilde{\mathbf{N}}_-^{(1)} \tag{33}$$

$$\tilde{\nabla}^2\tilde{\Psi}^{(1)} = \frac{1}{2}\left(\tilde{C}_-^{(1)} - \tilde{C}_+^{(1)}\right) \tag{34}$$

First-order perturbation for axial flow

For the axial case the flow was unidirectional and the concentrations were independent of z. The only nonzero components of the perturbed ion fluxes and electric potential were $\tilde{\mathbf{N}}_{\pm,z}^{(1)}(x,y)$ and $\tilde{\Psi}^{(1)}(z)$, which decoupled the electrokinetic equations. Moreover, the axial components of the pressure and electrical potential gradients were spatially uniform and equal to the corresponding macroscopic gradients. Under these conditions the momentum equation simplified to

$$\left(\frac{\lambda}{\beta\Pi_0}\right)\left\langle\frac{dP}{dz}\right\rangle = \tilde{\nabla}^2\tilde{v}_z^{(0)} + \frac{1}{2}\left(\tilde{C}_-^{(0)} - \tilde{C}_+^{(0)}\right)\left(\frac{\lambda}{\beta\Psi_0}\right)\left\langle\frac{d\Psi}{dz}\right\rangle. \tag{35}$$

The ion fluxes for axial flow were evaluated from

$$\tilde{\mathbf{N}}_{+,z}^{(1)} = -\tilde{C}_+^{(0)}\frac{\lambda}{\beta\Psi_0}\left\langle\frac{d\Psi}{dz}\right\rangle + \alpha\tilde{C}_+^{(0)}\tilde{v}_z{}^{(0)} \tag{36}$$

$$\tilde{\mathbf{N}}_{-,z}^{(1)} = \tilde{C}_-^{(0)}\frac{\lambda}{\beta\Psi_0}\left\langle\frac{d\Psi}{dz}\right\rangle + \alpha\frac{D_+}{D_-}\tilde{C}_-^{(0)}\tilde{v}_z{}^{(0)}. \tag{37}$$

Boundary conditions

The boundary conditions for the perturbation problems are summarized in Table 1, where $\tilde{x} = x/\lambda$, $\tilde{y} = y/\lambda$, $\tilde{r} = r/\lambda$, $\tilde{B} = B/\lambda$, and r is a local radial coordinate centered on a

Table 1. Boundary Conditions for the Dimensionless Perturbation Problems

	$\tilde{y} = 0, \tilde{B}$	$\tilde{x} = \pm\tilde{B}$	$\tilde{r} = \tilde{r}_i$
Zeroth order	$\frac{\partial\tilde{\Psi}^{(0)}}{\partial\tilde{y}} = 0$	$\frac{\partial\tilde{\Psi}^{(0)}}{\partial\tilde{x}} = 0$	$\frac{\partial\tilde{\Psi}^{(0)}}{\partial\tilde{r}} = -\frac{\sigma_i\lambda}{\varepsilon\Psi_0}$
First-order transverse	$\frac{\partial\tilde{P}^{(1)}}{\partial\tilde{y}} = 0$ $v_y^{(0)} = 0$ $\tilde{N}_{\pm,y}^{(1)} = 0$ $\frac{\partial\tilde{\Psi}^{(1)}}{\partial\tilde{y}} = 0$	$\begin{bmatrix}\tilde{P}^{(1)}(\tilde{x} = +\tilde{B}) = 0\\ \tilde{P}^{(1)}(\tilde{x} = -\tilde{B}) = 1\end{bmatrix}$ $\tilde{v}_y^{(0)} = 0$ $\tilde{C}_{\pm}^{(1)} = 0$ $\begin{bmatrix}\tilde{\Psi}^{(1)}(\tilde{x} = +\tilde{B}) = 0\\ \tilde{\Psi}^{(1)}(\tilde{x} = -\tilde{B}) = 1\end{bmatrix}$	$\tilde{\mathbf{v}}^{(0)} = 0$ $\tilde{N}_{\pm,y}^{(1)} = 0$ $\frac{\partial\tilde{\Psi}^{(1)}}{\partial\tilde{r}} = 0$
First-order axial	$\frac{\partial\tilde{v}_z^{(0)}}{\partial\tilde{y}} = 0$	$\frac{\partial\tilde{v}_z^{(0)}}{\partial\tilde{x}} = 0$	$\tilde{v}_z{}^{(0)} = 0$

given fiber. The conditions involving y and x arise mainly from symmetry and periodicity, respectively. For the transverse problem, the average pressure and electric field gradients across the unit cell (in the x direction) must equal the macroscopic gradients. Since the zeroth-order terms describe the equilibrium system, the macroscopic gradients must be related to the first-order terms. When an imposed pressure or potential gradient was desired, the upstream value of the corresponding perturbed variable was set to unity, as shown. Because of the linearity of Eq. 12, the values of the k_{ij} coefficients that we calculated were unaffected by the assumed magnitudes of the pressure and potential gradients. The fiber surface boundary conditions included no slip, no ion flux normal to the surface, and Gauss' law.

Evaluation of coupling coefficients

The coefficients in Eq. 12 were evaluated from the area-averaged velocity and current density in simulations in which there was either no applied pressure gradient or no applied potential gradient. With no pressure gradient, k_{12} and k_{22} were obtained; with no potential gradient, k_{11} and k_{21} were evaluated. For example, with $\langle\partial P/\partial x\rangle = 0$ (transverse) or $\langle\partial P/\partial z\rangle = 0$ (axial),

$$k_{22} = -\frac{\langle j_x\rangle}{\langle\partial\Psi/\partial x\rangle} = -\frac{F}{B\langle\partial\Psi/\partial x\rangle}\int_0^B (N_{+,x} - N_{-,x})\big|_{x=B}\, dy \quad \text{(transverse)} \quad (38)$$

$$k_{22} = -\frac{\langle j_z\rangle}{\langle\partial\Psi/\partial z\rangle} = -\frac{F}{2B^2\langle\partial\Psi/\partial z\rangle}\int_0^B\int_{-B}^B (N_{+,z} - N_{-,z})\, dx\, dy \quad \text{(axial)}. \quad (39)$$

All simulations were for aqueous NaCl solutions at room temperature: $\varepsilon = 7.08 \times 10^{-10}$ F/m, $\Psi_0 = RT/F = 2.5 \times 10^{-2}$ V, $\mu = 1.0 \times 10^{-3}$ Pa s, $D_+ = 1.3 \times 10^{-9}$ m^2/s, and $D_- = 2.0 \times 10^{-9}$ m^2/s. Other inputs are given in the figure legends.

Solution methods

A commercial finite element package (COMSOL Multiphysics™) was used to solve the system of perturbed differential equations. A mesh was generated with a higher density of nodes surrounding the fiber surfaces. The mesh was refined to provide convergence of the coupling coefficients to within 1%.

Results

Permeability for one fiber type

We begin by considering periodic arrays of a single type of charged fiber. The dashed curves in Figure 2 show the Darcy permeability as a function of the salt concentration in bulk solution, for either axial or transverse flow. In either case, κ increased with increasing salt concentration, reaching a plateau at high values of C_0. The Darcy permeability for axial flow was more sensitive to the salt concentration, and the plateau value was twice that for transverse flow. At high C_0, where the charge on the fiber surfaces is fully screened, κ should approach that for an uncharged system. This was confirmed by comparisons with previous analytical results, shown by the solid lines. For neutral fibers, the expression for axial flow is that of Drummond and Tahir,[5]

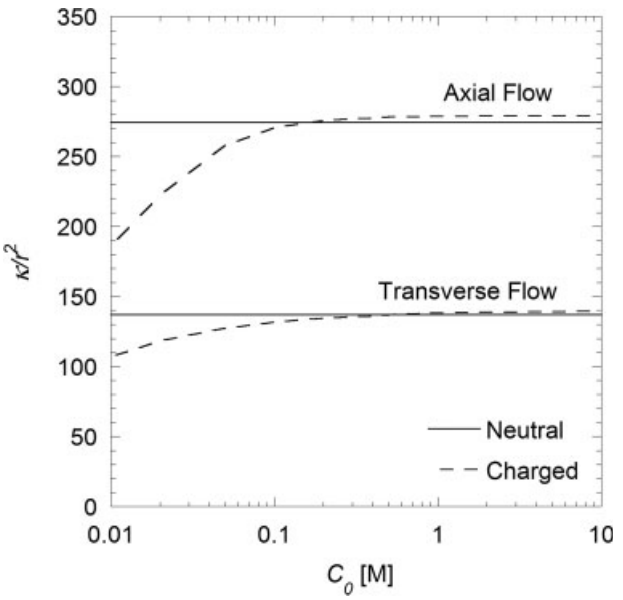

Figure 2. Dimensionless Darcy permeability of a square array of fibers of uniform size and charge, for either axial or transverse flow.

The parameter values were $\phi = 0.00375$, $r = 0.5$ nm, and $\sigma = -0.12$ C/m^2. The lines for neutral fibers are based on Eqs. 40 and 41.

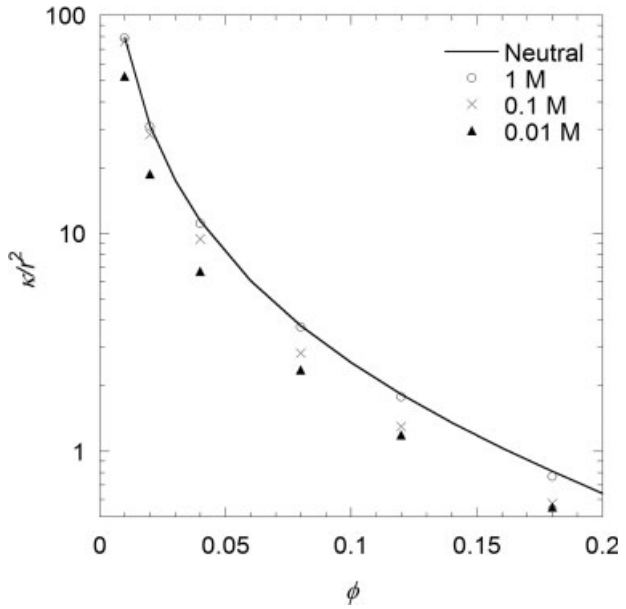

Figure 3. Dimensionless Darcy permeability for axial flow through uniform, square arrays of charged or neutral fibers, as a function of fiber volume fraction.

The results for charged fibers were obtained for three salt concentrations, with $r = 0.9$ nm and $\sigma = -0.12$ mC/m^2; those for neutral fibers are from Eq. 40.

$$\frac{\kappa}{r^2} = \frac{1}{4\phi}\left[-\ln\phi - 1.476 + 2\phi - 0.5\phi^2 + O\left(\phi^4\right)\right], \qquad (40)$$

and that for transverse flow is from Sangani and Acrivos,[7]

$$\frac{\kappa}{r^2} = \frac{1}{8\phi}\left[-\ln\phi - 1.476 + 2\phi - 1.774\phi^2 + 4.076\phi^3 + O\left(\phi^4\right)\right]. \qquad (41)$$

For $C_0 > 1$ M, the numerical results in Figure 2 are within 2% of those from Eqs. 40 and 41.

The dependence of κ on fiber volume fraction is shown in Figure 3, in which the results for axial flow past charged fibers at three salt concentrations are compared with those for neutral fibers. In all cases κ declined sharply with increasing ϕ. For $C_0 = 1$ M, the results for charged fibers were indistinguishable from those calculated from Eq. 40. The decline in κ with decreasing C_0 was more pronounced at the higher fiber volume fractions. At $C_0 = 0.1$ M, little or no effect of charge was evident for dilute fiber arrays ($\phi \leq 0.02$), but there was a 30% reduction in permeability for $\phi \geq 0.12$. At $C_0 = 0.01$ M, the charge effects were evident over the entire range of volume fractions examined.

Permeability for two fiber types

Flow through a two-fiber array was simulated for systems with an equal number of charged and uncharged fibers. Results are shown in Figure 4 for two representative situations, one with equal fiber radii and the other with unequal radii. The total fiber volume fraction and total fiber length per volume was the same in both cases. At any given salt concentration, and for either axial or transverse flow, κ for differing fiber radii was always slightly higher than that for equal radii. As C_0 was decreased from 1 to 0.01 M, the permeability declined by 10–22%.

The effects of a nonuniform charge density are illustrated in Figure 5. In these simulations the fiber radii were equal, and the fibers were either uniformly charged ("1 Fiber") or a mixture in which half was charged and half uncharged ("2 Fibers"). In this plot, the open-circuit Darcy permeability is expressed relative to the value for an uncharged system (κ_0). As noted earlier, electrokinetic coupling always reduces the apparent permeability, so that $\kappa/\kappa_0 \leq 1$ for all conditions shown. Whereas at high salt concentrations, κ/κ_0 decreased monotonically with increasing ϕ, at low salt concentrations it first decreased and then increased. The reason for the minimum in κ/κ_0 at low salt concentrations is discussed later. Note that while the two-fiber system contained half the total charge of the single-fiber one, the charge-related decrease in permeability in the former was not simply half that of the latter.

Mixing rules for Darcy permeability

The mixing rules given by Eqs. 8–11 were applied to several cases where simulation data were available, including results from the literature for neutral fibers and those computed by us for charged fibers. Equations 40 and 41 were employed when results were needed for periodic arrays of

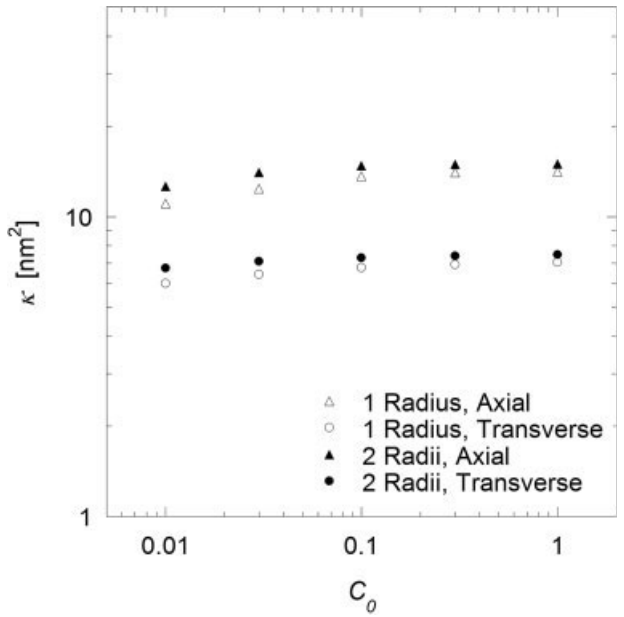

Figure 4. Darcy permeability of mixed arrays of charged and neutral fibers, as a function of salt concentration.

Circles are for transverse flow; triangles are for axial flow. For the array with a single radius (open symbols), $r_1 = r_2 = 1.2$ nm. For the array with two radii (filled symbols), $r_1 = 0.5$ nm and $r_2 = 1.6$ nm. In both systems, $\sigma_1 = -0.12$ C/m^2, $\sigma_2 = 0$, and $\phi = 0.044$. The fiber length per volume was 1.0×10^{12} cm/mL for both systems.

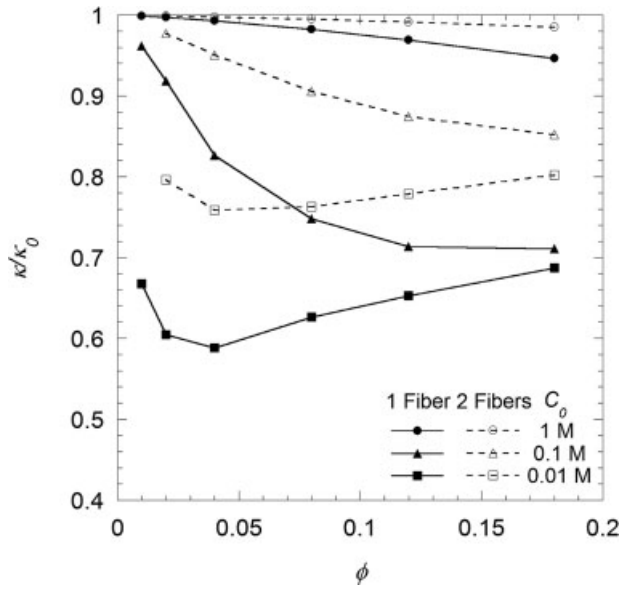

Figure 5. Darcy permeability for axial flow through two arrays containing charged fibers, as a function of total fiber volume fraction.

The permeability is expressed relative to that of an otherwise identical neutral array (κ_0). Filled symbols are for uniformly charged fibers with $r = 0.9$ nm and $\sigma = -0.12$ C/m^2 ("1 Fiber"). Open symbols are for a two-fiber array with $r_1 = r_2 = 0.9$ nm, $\sigma_1 = -0.12$ C/m^2, and $\sigma_2 = 0$ ("2 Fibers"). The neutral permeability was calculated using Eq. 40.

uniform, neutral fibers. For periodic arrays of charged fibers of uniform properties, we used our own model with $r_2 = 0$. For randomly oriented arrays of uniform, neutral fibers, we used an expression given by Clague et al.,[9]

$$\frac{\kappa}{r^2} = \left[\frac{1}{2}\sqrt{\frac{\pi}{\phi}} - 1\right]^2 [0.71407\ \exp(-0.51854\phi)] \qquad (42)$$

which is an empirical fit to their numerical results.

Permeability calculations for arrays of randomly oriented fibers can be approached as a kind of mixing problem, using the idealization that one-third of the fiber population is aligned parallel to each of the Cartesian axes.[14,18] For flow along a coordinate axis, this idea yields a binary mixture in which two-thirds of the fibers have a transverse orientation and one-third have an axial orientation. The performance of the mixing rules in this situation is illustrated in Figure 6, in which the various predictions are compared with Eq. 42 and with the numerical results of Clague and Phillips.[10] [There are some minor clarifications and corrections in Clague and Phillips,[10] provided to us by the authors: the permeability in their Figure 9 was scaled by r_2^2; the label of the ordinate in their Figure 10 should be k (nm^2), not k/r^2; and the ordinate in their Figure 11 should be labeled 0.1–10, not 1–100.] For small fiber volume fractions, the unweighted resistivity was slightly more accurate than the volume-weighted resistivity or volume-weighted permeability, whereas for large volume fractions there was not a clear favorite. Results for the length-weighted resistivity are not shown, because with equal fiber radii it is identical to the volume-weighted resistivity. We are unaware of any published results for randomly oriented charged fibers.

Results for a bimodal mixture of neutral fibers of differing radii are presented in Figure 7. In this case the "data" are provided by simulations of Clague and Phillips[10] for randomly oriented fine and coarse fibers, where the respective radii were 1.5 and 4.5 nm and the fibers were 87% fine and 13% coarse, by number. The unweighted resistivity was again slightly more accurate than the other mixing rules, with the volume-weighted resistivity a close second. The volume-weighted permeability and length-weighted resistivity each gave much larger errors.

Figure 8 compares the mixing rules with our own simulations for a mixture of charged and neutral fibers, over a range of salt concentrations. For this plot the fibers had equal radii, so that the mixing rules differed only in their treatment of fiber charge, not fiber size. In this case, the volume-weighted resistivity and volume-weighted permeability were each quite accurate, whereas the unweighted resistivity gave large errors. This was true for both axial and transverse flow.

In addition to the three examples just discussed, the mixing rules were compared to other data for neutral fibers with two radii,[10] as well as our simulations for mixtures of neutral and charged fibers with different radii, total volume fraction, and salt concentration. Figure 9 summarizes all of the results, as a plot of actual ("simulation") vs. predicted ("mixing rules") Darcy permeability. As indicated by the scatter around the identity line, the volume-weighted resistivity had

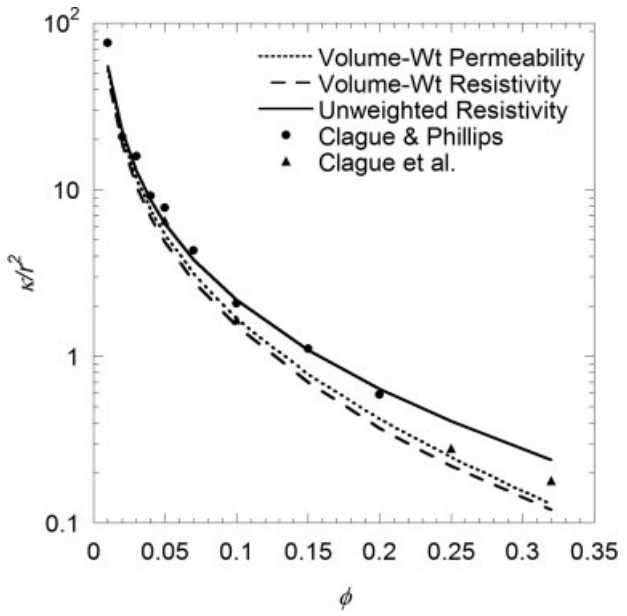

Figure 6. Dimensionless Darcy permeability of randomly oriented fibers of uniform radius.

Calculations with the three mixing rules used Eq. 40 for axial flow and Eq. 41 for transverse flow; the volume fractions for the two orientations were $\phi/3$ and $2\phi/3$, respectively. For this situation with uniform radii, results for the length-weighted resistivity (not shown) are identical to those for the volume-weighted resistivity. Symbols for the permeability of randomly oriented fibers are from numerical simulations by Clague and Phillips[10] and Clague et al.[9]

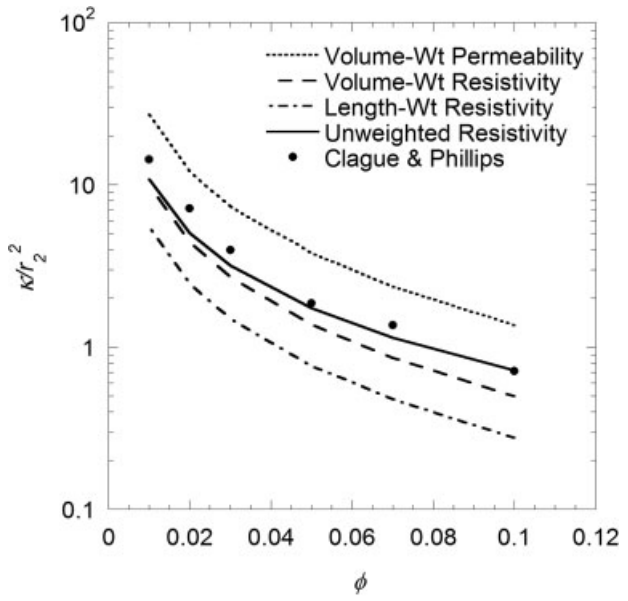

Figure 7. Dimensionless Darcy permeability of a randomly oriented array of fibers with two radii.

The radii are $r_2 = 4.5$ nm ("coarse") and $r_1 = 1.5$ nm ("fine"), and the mixture is 13% coarse and 87% fine, by number. Calculations for the four mixing rules used Eq. 42 for a randomly oriented array of fibers with one radius. Symbols denote numerical simulations from Clague and Phillips.[10]

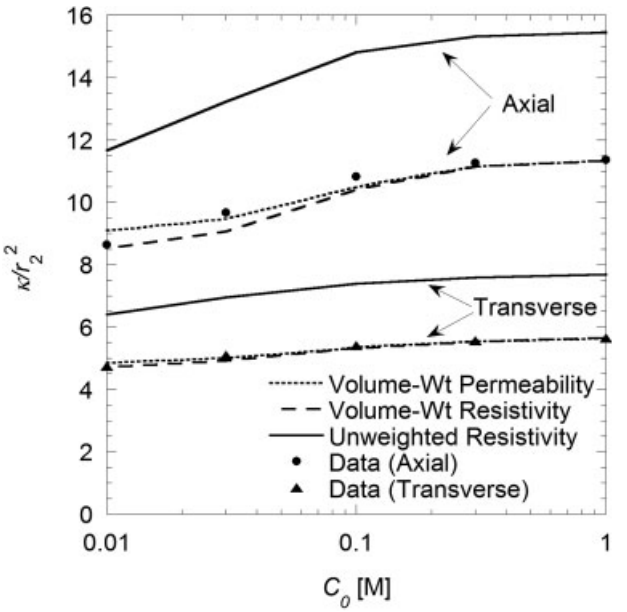

Figure 8. Dimensionless Darcy permeability of an array with an equal number of charged and neutral fibers of uniform size, as a function of salt concentration.

Results are shown for both axial and transverse flow. The parameters used were $r_1 = r_2 = 0.9$ nm, $\phi_1 = \phi_2 = 0.02$, $\sigma_1 = -0.12$ C/m^2, and $\sigma_2 = 0$. Calculations for the three mixing rules used Eqs. 40 and 41 for periodic arrays of neutral fibers and the double-layer model for periodic arrays of charged fibers. Symbols are "exact" results for the mixed array, also computed using the present double-layer model.

the fewest large errors, suggesting that it is the most reliable overall. This impression is confirmed by the results in Table 2, which gives the root-mean-square (rms) errors of the four mixing rules for all 64 cases examined; these are relative errors, normalized by the simulation values. The volume-weighted resistivity had the lowest rms error for both neutral and charged systems. Its overall error of 24% was considerably lower than those for the other mixing rules, which ranged from 40 to 128%.

Discussion

In evaluating the accuracy of the various mixing rules for fibrous media, we found it desirable to augment the Darcy permeabilities reported in the literature with new calculations involving charged fibers. The model we employed had a spatially periodic arrangement of two types of fibers (Figure 1), which could differ in radius and/or surface charge density. For the special case of a single-fiber type (obtained by setting $r_2 = 0$), the present model is equivalent to one that was used to compute electrokinetic coupling coefficients for an extracellular matrix.[8,19] The coefficients we obtained were generally in excellent agreement with the previous results (<4% difference). A larger (30%) discrepancy between the values for k_{22} for axial flow was found to be exactly accounted for if the prior results omitted the migration terms in the ion fluxes. Also, as shown in Figures 2 and 3, our finite element calculations agreed well with previous analytical results for uncharged fibers.

It was shown in Figure 4 that, when the fiber volume fraction and total fiber length per unit volume were held

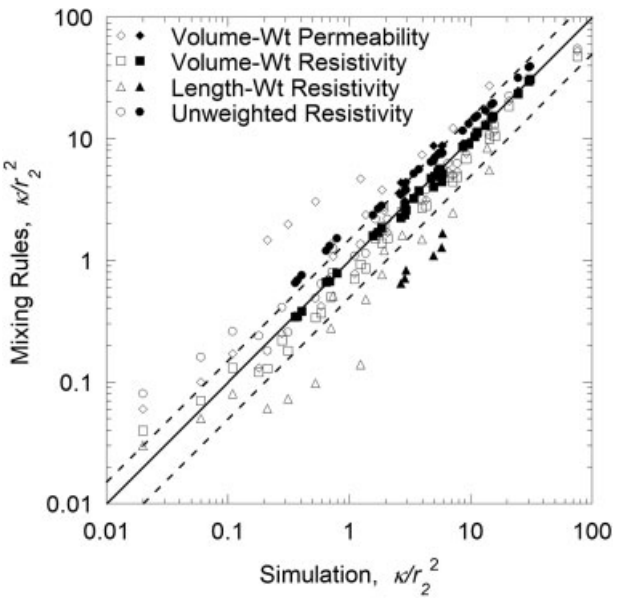

Figure 9. Dimensionless Darcy permeability of complex fiber systems, as predicted by mixing rules or computed from multifiber simulations.

The solid line corresponds to equality of the two results and the dashed lines represent ±50% deviations. Open symbols are data for neutral fiber systems from the literature[9,10] and solid symbols are data for charged fiber systems from the present work.

constant, the Darcy permeability of a charged fiber system with differing radii was almost identical to that of a system with uniform radii. This is consistent with expectations from slender body theory for neutral objects, which predicts that the hydraulic permeability depends mainly on the total length per volume.[10] In both systems, there was approximately a 15% reduction in the hydraulic permeability at 0.01 M compared to neutral conditions. This suggests that a mixture of two fiber radii might be modeled accurately as one with a single effective radius. Although true for the conditions of Figure 4, where in the bimodal system the radii differed by only a factor of 3, such an approximation is questionable for charged fibers if the radii are highly dissimilar. The problem with using an effective radius for a mixture of charged fibers is that radius adjustments can strongly influence surface charge densities.

The minimum in κ/κ_0 that is seen in Figure 5 at the lowest salt concentration reflects a competition between the effects of ϕ on κ_0 and its effects on the electrical body force. Qualitatively similar behavior is predicted by a model based on Donnan equilibria, in which the microstructure is ignored and the fibrous material is characterized only by a concentration C_m of fixed negative charges.[1] Because the Donnan approach yields a simple analytical result, it provides the clearest explanation for the minimum in κ/κ_0. For equal cation and anion diffusivities ($D_\pm = D$), the Donnan result is

$$\frac{\kappa}{\kappa_0} = \frac{1}{1+\kappa_0\gamma} \tag{43}$$

$$\gamma = \frac{RTC_m^2}{\mu D\sqrt{C_m^2 + 4C_0^2}} \tag{44}$$

For the conditions of Figure 5, where fiber radius and surface charge density are both fixed, $C_m \propto \phi$. Thus, from Eq. 44, $\gamma \propto \phi^2$ for a weakly charged fiber matrix ($C_m << 2C_0$), a condition that is reached inevitably as $\phi \to 0$. As shown by Eqs. 40 or 41, $\kappa_0 \propto -\ln \phi/\phi$ to leading order. Accordingly, $\kappa_0\gamma$ will vary as $-\phi \ln \phi$ for small enough ϕ. Because the values of this function increase from zero to a maximum positive value and then decline, it follows from Eq. 43 that κ/κ_0 will sometimes have a minimum at a certain value of ϕ. Below that fiber volume fraction, the dominant effect of increasing ϕ is the increase in C_m, which amplifies the electrical force opposing the flow; above it, the main effect is the decrease in κ_0 as the fibers become more concentrated. For the conditions of Figure 5, only for $C_0 = 0.01$ M does the minimum in κ/κ_0 occurs at a value of ϕ that is small enough to be of interest. Of course, the smaller the salt concentration, the smaller is the value of ϕ needed to make the charge on the fiber matrix relatively weak. If ϕ becomes large enough to make the fiber matrix highly charged ($C_m >> 2C_0$), then $\kappa_0\gamma \propto -\ln \phi$ and κ/κ_0 will increase even more rapidly with increasing ϕ.

The four mixing rules tested here have each been employed for particular purposes in the literature, but generally without comparisons with one another. Most have simple macroscopic interpretations. The volume-weighted permeability is what would be obtained if the two types of fibers occupied separate, parallel phases in a slab of fibrous material, with a fiber volume fraction ϕ in each and an area fraction ϕ_i/ϕ. The volume-weighted resistivity is equivalent to layers in series, with a volume fraction ϕ in each and a layer thickness proportional to ϕ_i. The length-weighted resistivity is equivalent to layers in series with each thickness proportional to the total fiber length, or ϕ_i/r_1^2. Only the unweighted resistivity seems to have no macroscopic analog.

Table 2. Root-Mean-Square Errors of Darcy Permeabilities Predicted by the Mixing Rules

	Volume-weighted Permeability	Volume-weighted Resistivity	Length-weighted Resistivity	Unweighted Resistivity
Neutral ($n = 30$)	1.86	0.33	0.48	0.69
Charged ($n = 34$)	0.24	0.08	0.32	0.49
Total ($n = 64$)	1.28	0.24	0.40	0.59

Results for neutral and charged fibers are tabulated, along with those obtained overall. The errors are relative (fraction of "exact" value from simulation).

One difference among the mixing rules is what they imply about the interactions between a fiber and its neighbors. Most base the calculation of κ_i on the total volume fraction ϕ, which is equivalent to assuming that all fibers in the mixture have the same effect on the resistivity of fiber type i. However, the unweighted resistivity bases κ_i on ϕ_i, assuming in effect that fibers of type i are influenced preferentially by those of the same type. This bias in favor of like fibers seems to cause problems in systems where at least some fibers are charged, as that is where the unweighted resistivity performed worse than the other mixing rules (Table 2). Another noteworthy difference is that, if both fiber types are identical [i.e., $r_1 = r_2$ and $\kappa_1(\phi) = \kappa_2(\phi)$], the unweighted resistivity does not reduce correctly to the single-fiber expression, whereas the other mixing rules do.

Of the three kinds of "mixing processes" considered—involving different orientations, radii, or charge densities—orientation effects seem easiest to capture. This is indicated by the results in Figure 6, where the maximum error for any of the mixing rule predictions was only 40%. Underlying the forgiving nature of orientation-averaging is the fact that κ values for axial and transverse flow differ by only a factor of 2 (for neutral systems). The differences between the mixing rules were more apparent when the permeabilities of the fiber populations were very different, such as in Figure 7, where the threefold difference in fiber radii implies a ninefold difference between $\kappa_1(\phi)$ and $\kappa_2(\phi)$. Although the Darcy permeability tends to be less sensitive to charge density than to fiber radius, the results in Figure 8 [where the differences in charge density created up to 1.5-fold differences between $\kappa_1(\phi)$ and $\kappa_2(\phi)$] also clearly discriminated among the mixing rules. Among the 64 cases where we made comparisons (as summarized in Figure 9), the length-weighted resistivity tended to underestimate the permeability of many systems, including those with charged fibers. The volume-weighted permeability and unweighted resistivity had a tendency to overestimate the permeability of both charged and neutral systems. Overall, the volume-weighted resistivity appeared to be the most reliable method for predicting the Darcy permeability of complex systems, includ-

ing mixtures of fibers of differing orientation, radius, and/or charge density.

Except for situations in which its macroscopic analog might be realized (e.g., fiber types segregated from one another in parallel or series layers), none of the mixing rules has a rigorous theoretical basis. Thus, any conclusions about their relative accuracy are necessarily empirical, and dependent on the choice of data. Although we created a data set that is sizable enough to represent a fairly wide variety of situations, additional results would be informative. For example, we were unable to test the efficacy of the mixing rules for orientation-averaging of charged fibers, because there are no simulation results at present for arrays of randomly oriented charged fibers. Also, there appear to be no results yet for mixtures containing three or more fiber types. However, based on the information at hand, the volume-weighted resistivity seems most reliable. Over a range of situations in which there were sometimes several-fold differences among the mixing rule predictions, it gave a rms error of only 24%. Thus, Eq. 8 seems to provide the best way to estimate the Darcy permeabilities of complex fiber mixtures from the composition of the mixture and the properties of the individual fiber types.

Literature Cited

1. Deen WM, Satvat B, Jamieson JM. Theoretical model for glomerular filtration of charged solutes. *Am J Physiol*. 1980;238:F126–F139.
2. Edwards A, Daniels BS, Deen WM. Hindered transport of macromolecules in isolated glomeruli. II. Convection and pressure effects in basement membranes. *Biophys J*. 1997;72:214–222.
3. Maroudas A, Mizrahi J, Haim EB, Ziv I. Swelling pressure in cartilage. In: Staub N, Hogg J, Hargens A, editors. Intersitional-Lymphatic Liquid and Solute Movement, Vol. 13. Basel, Switzerland: Karger, 1987:203–212.
4. Levick JR. Flow through interstitium and other fiberous matrices. *Q J Exp Physiol*. 1987;72:409.
5. Drummond JE, Tahir MI. Laminar viscous flow through regular arrays of parallel solid cylinders. *Int J Multiphase Flow*. 1984;10:515–540.
6. Jackson GW, James DF. The permeability of fibrous porous media. *Can J Chem Eng*. 1986;64:364–374.
7. Sangani AS, Acrivos A. Slow flow past periodic arrays of cylinders with application to heat transfer. *Int J Multiphase Flow*. 1982; 8:193–206.
8. Chammas P, Federspiel WJ, Eisenberg SR. A microcontinuum model of electrokinetic coupling in the extracellular matrix: perturbation formulation and solution. *J Colloid Interface Sci*. 1994;168: 526–538.
9. Clague DS, Kandhai BD, Zhang R, Sloot PMA. Hydraulic permeability of (un)bounded fibrous media using the lattice Boltzmann method. *Phys Rev E: Stat Nonlin Soft Matter Phys*. 2000;61:616–625.
10. Clague DS, Phillips RJ. A numerical calculation of the hydraulic permeability of three-dimensional disordered fibrous media. *Phys Fluids A*. 1997;9:1562–1572.
11. Spielman L, Goren SL. Model for predicting pressure drop and filtration efficiency in fibrous media. *Environ Sci Technol*. 1968;2: 279–287.
12. Edwards DA, Shapiro M, Bar-Yoseph P, Shapira M. The influence of Reynolds number upon the apparent permeability of spatially periodic arrays of cylinders. *Phys Fluids A*. 1990;2:45–55.
13. Ethier CR. Flow through mixed fibrous porous materials. *AIChE J*. 1991;37:1227–1236.
14. Jackson GW, James DF. The hydrodynamic resistance of hyaluronic acid and its contribution to tissue permeability. *Biorheology*. 1982; 19:317–330.
15. Eisenberg SR, Grodzinsky AJ. Electrokinetic micromodel of extracellular matrix and other polyelectrolyte networks. *Physico Chem Hydrodyn*. 1988;10:517–539.
16. Ethier CR. *Hydrodynamics of Flow through Gels with Applications to the Eye*, SM Thesis. Cambridge, MA: Department of Mechanical Engineering, Massachusetts Institute of Technology, 1983.
17. Onsager L. Theories and problems of liquid diffusion. *Ann NY Acad Sci*. 1945;96:241–265.
18. Stigter D. Electrophoresis of highly charged colloidal cylinders in univalent salt solutions. I. Random orientation in external field and application to polyelectrolytes. *J Phys Chem*. 1978;82:1424–1429.
19. Chammas P. *Electromechanical Coupling in Articular Cartilage: An Electrokinetic Micromodel and Experimental Results*, SM Thesis. Boston, MA: Department of Biomedical Engineering, Boston University, 1989.

Manuscript received Jun. 27, 2007, and revision received Sept. 20, 2007.